ACS APPLIED MATERIALS & INTERFACES

Research Article

www.acsami.org

Relaxor Ferroelectricity and Magnetoelectric Coupling in ZnO−Co Nanocomposite Thin Films: Beyond Multiferroic Composites

D. Y. Li,[†] Y. J. Zeng,*[,†] D. Batuk,[§] L. M. C. Pereira,[‡] Z. Z. Ye,[∥] C. Fleischmann,[‡] M. Menghini,[†] S. Nikitenko,[⊥] J. Hadermann,[§] K. Temst,[‡] A. Vantomme,[‡] M. J. Van Bael,[†] J.-P. Locquet,[†] and C. Van Haesendonck[†]

[†]Laboratory of Solid-State Physics and Magnetism and [‡]Instituut voor Kern-en Stralingsfysica, KU Leuven, Celestijnenlaan 200 D, BE-3001 Leuven, Belgium

[§]Electron Microscopy for Materials Science − EMAT, University of Antwerp, Groenenborgerlaan 171, BE-2020 Antwerp, Belgium

[∥]State Key Laboratory of Silicon Materials, Department of Materials Science and Engineering, Zhejiang University, Hangzhou 310027, P. R. China

[⊥]Netherlands Organization for Scientific Research (NWO), DUBBLE@ESRF, 6 rue Jules Horowitz, 38043 Grenoble, France

Supporting Information

ABSTRACT: ZnO−Co nanocomposite thin films are synthesized by combination of pulsed laser deposition of ZnO and Co ion implantation. Both superparamagnetism and relaxor ferroelectricity as well as magnetoelectric coupling in the nanocomposites have been demonstrated. The unexpected relaxor ferroelectricity is believed to be the result of the local lattice distortion induced by the incorporation of the Co nanoparticles. Magnetoelectric coupling can be attributed to the interaction between the electric dipole moments and the magnetic moments, which are both induced by the incorporation of Co. The introduced ZnO−Co nanocomposite thin films are different from conventional strain-mediated multiferroic composites.

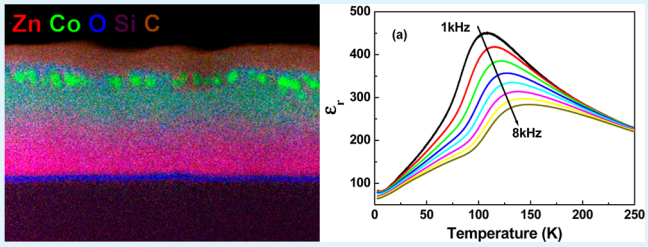

KEYWORDS: *multiferroics, magnetoelectric coupling, relaxor ferroelectricity, nanocomposite, ion implantation*

1. INTRODUCTION

Multiferroics and magnetoelectrics have attracted considerable attention during the last few years.[1−5] In spite of the intrinsic difficulties, many stimulating results have been reported on various material systems and mechanisms.[6−8] In particular, thin-film multiferroics are attractive because of the convenience to combine multiferroic properties with other unique properties associated with thin-film physics.[1,9] However, it remains very challenging to fabricate single-phase multiferroic thin films, which are normally complex oxides containing at least three elements. Without a delicate process control, a second phase is likely to appear, which can degrade or even erase the desired properties.[10] In addition, the sensitivity of these complex oxides to the strain, stoichiometry, oxidation state, disorder, and so forth may lead to drastic modifications of their electronic and magnetic properties at the nanoscale.[11] Multiferroic composites, proposed years ago as an alternative, have less limitations with respect to the sample preparation. The most frequently proposed multiferroic composite is a ferromagnetic phase embedded or layered in a ferroelectric matrix and typically based on the mechanical strain-mediated mechanism (magnetostriction and piezoelectricity), where the coupling is induced by elastic deformation through the interface strain.[11−13] As ferromagnetism and ferroelectricity appear in different phases, composites avoid the fundamental problem related to the mutual exclusion of ferromagnetism and ferroelectricity, which is considered to be the main obstacle occurring in phase-pure multiferroic materials.[14]

Here, we introduce an alternative route to prepare thin-film multiferroic nanocomposites, in which the complex ferroelectric matrix is replaced by a simple ZnO thin film. ZnO, by virtue of its excellent material properties, including a wide direct bandgap of 3.37 eV at room temperature, a large exciton binding energy of 60 meV, the availability of high-quality bulk crystals, as well as high electron mobility and high thermal conductivity, has attracted particular attention as a revival semiconductor.[15] At the same time, ZnO is a "famous" piezoelectric material, which is more environmentally friendly than most ferroelectric materials, and has been used as main component in piezotronics and piezophototronics.[16] We have recently developed a reliable route to tune the magnetic as well as the electrical properties of ZnO by using ion implantation.[17,18] In this study, we rely on pulsed laser deposition (PLD) of ZnO and on Co ion implantation to obtain ZnO−Co nanocomposite thin films. We observe both superparamagnetism and relaxor ferroelectricity, as well as magnetoelectric

Received: November 26, 2013
Accepted: March 5, 2014
Published: March 5, 2014

   dx.doi.org/10.1021/am4053877 | ACS Appl. Mater. Interfaces 2014, 6, 4737−4742

coupling in the composite films. The unexpected relaxor ferroelectric behavior is believed to be the result of the local lattice distortion induced by the incorporation of the Co nanoparticles (NPs). Unlike typical multiferroic composites, in which ferromagnetism and ferroelectricity come from different phases that are mixed into a composite, the ferroelectricity in our ZnO−Co is triggered by the ferromagnetic NPs. The ZnO−Co thin films therefore cannot be treated as a simple composite. Novel magnetoelectric coupling beyond the strain-mediated mechanism can be expected. Relaxor ferroelectricity, which is mostly observed in perovskite-related materials, results in unique physical properties including large dielectric susceptibilities and giant electromechanical response.[19−22] The relaxor ferroelectricity and magnetoelectric coupling in ZnO−Co makes this composite a promising candidate for relaxor multiferroics.

2. EXPERIMENTAL SECTION

ZnO thin films with a thickness of about 130 nm were grown by PLD on highly doped Si substrates. The growth temperature was 550 °C. The oxygen pressure was maintained at 0.1 Pa during the growth of ZnO. The energy density per pulse was estimated to be 3 J/cm^2. The substrate was located at a distance of 5 cm from the target. Co was successively implanted at a fluence of 1×10^{17} ions/cm^2 and an energy of 80 keV at room temperature. The ion implantation was done under a tilt angle of 10° to minimize ion channeling. The crystal structure of the sample was characterized by X-ray diffraction (XRD, PANalytical X'Pert PRO MRD system). The microstructure and elemental distribution of the sample were studied by transmission electron microscopy (TEM). A cross section specimen for TEM was prepared by slicing the sample perpendicular to the film surface. Energy filtered transmission electron microscopy (EFTEM) and energy dispersive X-ray (EDX) were conducted on Philips CM30-FEG and FEI Tecnai G2 microscopes operated at 300 and 200 keV, respectively. The local coordination environment of Co in the sample was characterized by X-ray absorption near edge structure (XANES) and extended X-ray absorption fine structure (EXAFS) at the DUBBLE (BM26) beamline of the European Synchrotron Radiation Facility (ESRF). CoO powder and metallic Co foil were used as the reference materials. Magnetic properties were measured with a superconducting quantum interference device magnetometer (SQUID, Quantum Design MPMS XL-5) following careful experimental procedures in order to minimize magnetic contamination and other experimental artifacts.[23] Good ohmic contact was formed by deposition of Au/Ti bilayer,[24] with a contact area of 0.4 mm^2. The temperature dependent electrical measurements were performed in a helium-4 flow cryostat with a superconducting magnet (Oxford Instruments). The magnetic field was applied parallel to the sample surface. The resistance was measured using a low-frequency ac resistance bridge (Stanford Research Systems SIM921). The dielectric measurements were performed using a Keithley 4200-SCS setup, and the polarization measurements were performed with a TF Analyzer 2000 from aixACCT Systems.

3. RESULTS AND DISCUSSION

As-grown ZnO thin films show a good crystalline quality with (002) preferential orientation. After Co ion implantation, XRD reveals the crystalline structure of the Co NPs as well as their parallel lattice alignment with respect to the ZnO host matrix. Using the Scherrer formula the average size of the NPs is calculated to be 7 nm (Supporting Information, Figure S1).

The distribution of Co over the sample is analyzed using EFTEM and EDX. In Figure 1, we present a bright field TEM image along with a colored map of the element distribution, which is obtained using the individual EFTEM maps for every constituent element (Supporting Information, Figure S2). The

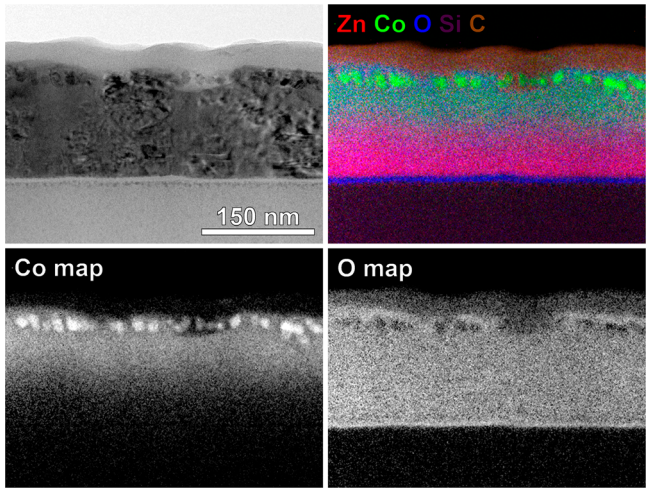

Figure 1. Bright field TEM image of a Co-implanted ZnO thin film (top-left), colored EFTEM map of the element distribution (top-right), Co EFTEM map (bottom-left), and O EFTEM map (bottom-right).

EFTEM reveals that Co is embedded into the ZnO film in two different forms, that is, as metallic Co NPs concentrated at the surface and as oxidized Co evenly distributed in the ZnO matrix.[18] The size of the Co NPs estimated from the TEM data is about 7−10 nm, which is consistent with the XRD results. The Co concentration gradually decreases upon going from the film surface to the substrate (Supporting Information, Figure S3). According to the EDX data, the overall Co concentration (Co/[Co + Zn]) is 32 ± 4 atom % and does not significantly vary across the sample.

The local coordination environment of the Co atoms in the ZnO matrix is characterised by XANES and EXAFS measurements. In Figure 2a, we present the XANES spectra of the Co K-edge for the Co-implanted ZnO thin film as well as for pure CoO and Co reference samples. The XANES of the Co-implanted ZnO resembles the results of CoO rather than of Co, indicating that the majority of the implanted Co is in the oxidized state. In particular, the appearance of a small pre-edge absorption at 7709 eV is due to transitions of Co 1s electrons to 4p-3d hybridized states, which become allowed by the nearly tetrahedral bonding of Co at the Zn sites within the wurtzite structure.[25] In Figure 2b, we plot the magnitude of the k^2-weighted Fourier transforms of the EXAFS spectra. For the Co-implanted ZnO, the spectrum reveals two dominant peaks related to the first O shell and second Zn shell in the wurtzite model. This indicates that the majority of the Co atoms are located at Zn sites. On the other hand, a small peak appears at the same position as the first dominant peak in the spectrum of the Co reference sample, which is related to the first Co shell in the Co metal. This suggests that the latter Co atoms are metallic and most probably belong to the Co NPs imaged by TEM. From the above-mentioned structural characterization, we conclude that the majority of the implanted Co atoms are located at Zn sites bonding to the O, while part of the implanted Co atoms form metallic Co NPs. The system can be described as consisting of Co NPs embedded in a (Zn,Co)O matrix.

Figure 3a presents the zero-field-cooled/field-cooled (ZFC/FC) magnetization curves. Below 300 K, the splitting between the ZFC and FC magnetization curves demonstrates the typical behavior of a superparamagnetic system.[26] Each NP will have

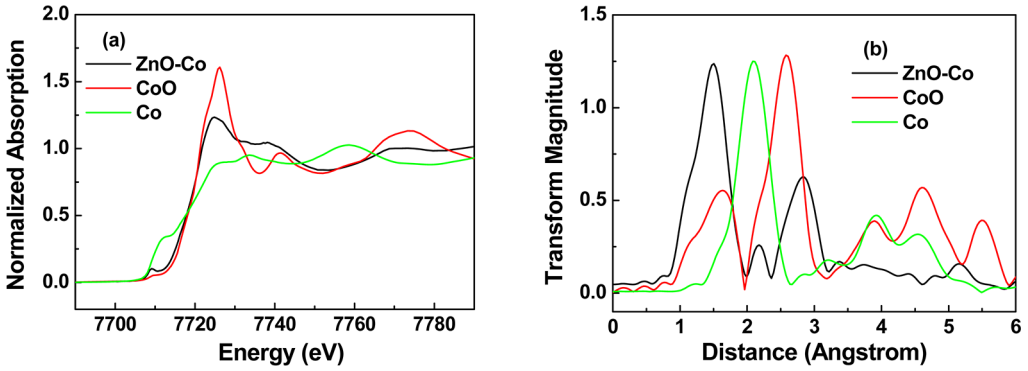

Figure 2. (a) Co K-edge XANES spectra of Co-implanted ZnO thin films, CoO, and Co metal. (b) Magnitude of the k^2-weighted Fourier transforms of the EXAFS spectra. For clarity, the magnitude of CoO and Co is multiplied by 0.5 and 0.3, respectively.

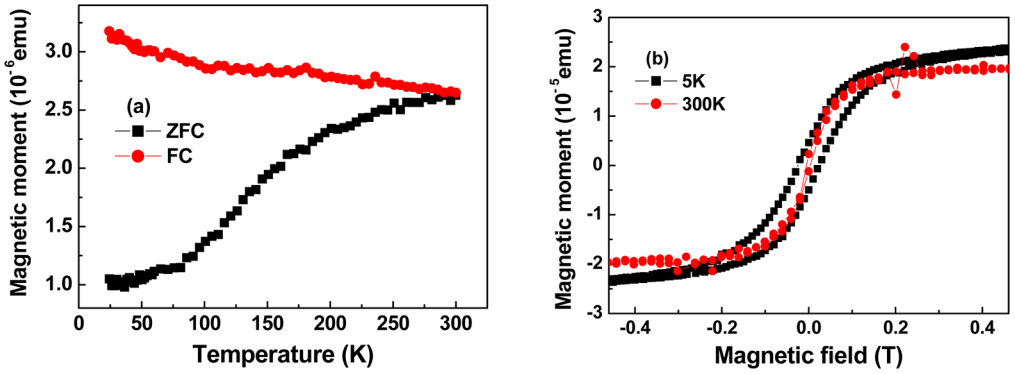

Figure 3. (a) ZFC/FC magnetization curves at a magnetic field of 0.01T. (b) $M-H$ hysteresis loop at 5 and 300 K.

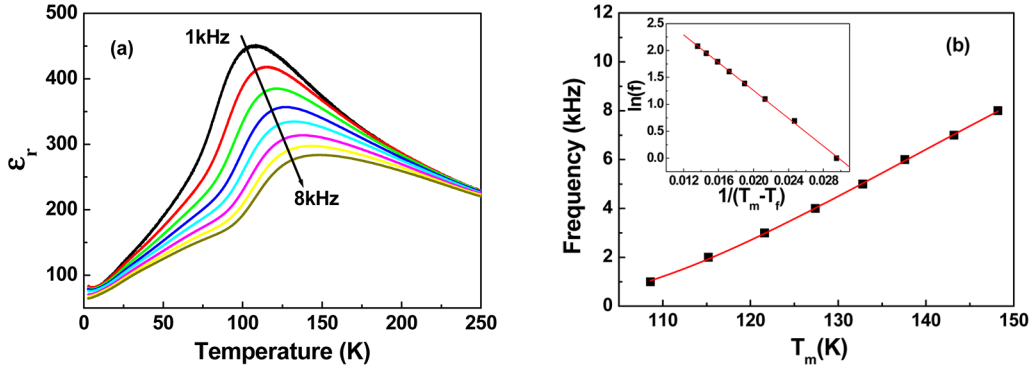

Figure 4. (a) Frequency-dependent $\varepsilon_r(T)$ curves measured from 250 to 2 K. (b) Frequency as a function of T_m obtained from (a). The red curve represents the least-squares fitting using the Vogel–Fulcher relation. The inset illustrates the linear dependence of $\ln(f)$ on $1/(T_m - T_f)$.

its characteristic blocking temperature T_B. Our system consists of NPs with a distribution of sizes, which appears in the ZFC/FC magnetization curves as a gradual curvature around T_B rather than as a sharp peak. In Figure 3b, the field dependent magnetization ($M-H$) curves confirm the superparamagnetic behavior. At 300 K, the $M-H$ curve shows a saturation moment with negligible coercivity. On the other hand, below T_B (5 K), a transition to ferromagnetism is observed with increased coercivity and remanence. The observed superparamagnetic behaviour is consistent with the TEM observations, which demonstrate the presence of Co NPs embedded in the (Zn,Co)O matrix.

In Figure 4a, we present the temperature dependence of the dielectric constant ε_r of Co-implanted ZnO at different frequencies. Key features are (i) very large dielectric constants compared to bulk ZnO (typically below 10), (ii) a very broad peak in the $\varepsilon_r(T)$ curve with a peak value at T_m, and (iii) a frequency dependent T_m with T_m shifting to a higher temperature when the frequency increases. These characteristic behaviors as well as the large dielectric constant are consistent with the formation of relaxor ferroelectricity.[19−22] Instead of the sharp phase transition at the Curie temperature that occurs in classical ferroelectric materials, a broadened phase transition is expected to occur in relaxor ferroelectrics.[19,20,27,28] As illustrated in Figure 4a, a very broad dielectric peak appears between 100 and 150 K, which corresponds to a series of dynamic transition temperatures T_m.

Empirically, the relaxation dynamics of a relaxor can be described by the Vogel–Fulcher (V–F) relation:[28,29]

dx.doi.org/10.1021/am4053877 | ACS Appl. Mater. Interfaces 2014, 6, 4737−4742

$$\tau = \tau_0 \exp\left[\frac{U}{k_B(T - T_f)}\right]$$

where τ_0 is the inverse attempt frequency, U is the activation energy, and T_f is the static freezing temperature. τ and T correspond to the reciprocal of the measurement frequency and to T_m, respectively. The least-squares fitting in Figure 4b reveals a good agreement with the experimental data, resulting in the fitting parameters $f_0 = 46 \pm 4$ kHz (corresponding to $\tau_0 = 2.2 \times 10^{-5}$ s), $U/k_B = 128 \pm 10$ K, and $T_f = 75 \pm 2$ K. The inset of Figure 4b illustrates the linear dependence of $\ln(f)$ on $1/(T_m - T_f)$, which further confirms the validity of the fitting in terms of the V−F relation.

The physical origin of the relaxor behavior is a network of polar nanoregions (PNRs) embedded in a highly polarizable matrix. In our system of Co-implanted ZnO, a qualitative physical picture can be drawn. High-fluence ion implantation induces a certain level of compositional or crystalline disorder, which results in electric dipoles embedded in the highly polarizable (Zn,Co)O matrix. Upon cooling, a network of randomly interacting dipolar entities starts to develop and to form PNRs. The PNRs polarize the surrounding medium within a correlation radius r_c, resulting in the formation of polarized clusters. With decreasing temperature, r_c increases because of the decreasing thermal fluctuations, and the polarized clusters grow and merge until a frozen state is reached. Within this simplified model, when the temperature starts to decrease, the PNRs will grow but r_c is not sufficiently large to form a correlated cluster, they behave like uncorrelated dipoles. ε_r then increases according to a "Curie−Weiss-like" law.[19,27] As the temperature further decreases, the increase of ε_r slows down owing to the growth of r_c and the enhanced correlation between the dipoles. In other words, the fluctuation of the interacting dipolar moments undergoes a dynamic slow-down, which is usually described in terms of a freezing process.[19,20,27,28] Finally, ε_r starts to decrease because of the lack of macroscopic polarizability. As a result, a broad peak appears in the $\varepsilon(T)$ curve. At a certain low temperature (freezing temperature), r_c becomes sufficiently large so that the clusters connect to each other or percolate throughout the whole sample. The system is fully frustrated and a frozen region with a turning point shows up in the $\varepsilon(T)$ curve.

To our surprise, the signature of such a transition process is also present in a simple measurement of the temperature dependence of the resistivity ($\rho-T$ curve). In Figure 5, we plot the $\rho-T$ curve of the Co-implanted sample, where a bump shows up in the 40−120 K interval. From this bump, two characteristic temperatures can be inferred, which separate regions with different transport mechanisms: Above 120 K, where $1/\rho \propto T^{3/2}$ (Supporting Information, Figure S4a), an impurity scattering mechanism dominates. Below 40 K, where $\rho(T) \propto \exp[(T_0/T)^{1/4}]$ (Supporting Information, Figure S4b), a variable-range hopping mechanism dominates.[30] It is interesting to point out that the previously discussed freezing temperature at 75 K derived from the V−F relation is located well within the 40−120 K interval where the bump in the $\rho-T$ curve occurs. We therefore believe that this bump reflects a transition not only for the electron transport mechanism but also for the relaxor behavior. At higher temperatures above 120 K, transport in a paraelectric-like state is dominated by impurity scattering, while at low temperatures below 40 K transport in a frozen state is dominated by variable-range hopping.

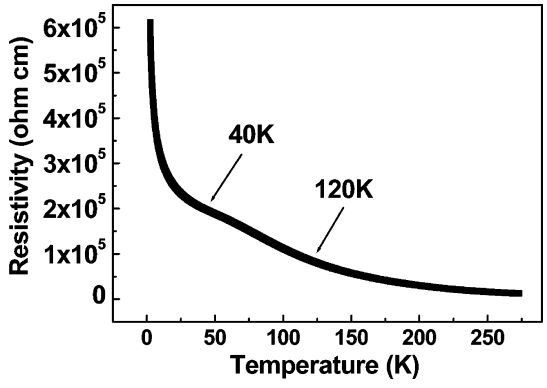

Figure 5. Resistivity of the Co-implanted ZnO thin film as a function of temperature.

Another characteristic feature of relaxor ferroelectrics is a slim polarization hysteresis loop ($P-E$ loop) when compared with classical ferroelectric materials.[19,27] A rather small remanent polarization P_r is expected in relaxor ferroelectrics due to the reorientation of the PNRs when removing the applied electrical field. In Figure 6b (black curve), we present a typical polarization hysteresis loop of Co-implanted ZnO measured at 5 K. The clear hysteresis loop, but with a slim shape, confirms the relaxor ferroelectric nature of our ZnO−Co system. In Figure 6a, we plot the temperature-dependent remanent polarization, where the remanent polarization is defined as $(P_{r+} - P_{r-})/2$ inferred from the $P-E$ hysteresis loop. Above 120 K, the remanent polarization is close to zero, suggesting a paraelectric-like state. Between 120 and 40 K, the remanent polarization increases almost linearly with decreasing temperature, which is due to the growth of the PNRs networks. The freezing temperature of 75 K derived from the V−F relation is located near the center of this temperature region. Finally, the remanent polarization stops increasing and remains almost constant below 40 K, which can be understood based on the fact that the system is fully frustrated below 40 K and has no more rotatable dipole moments. It should be emphasized that the polarization measurements, together with the temperature-dependent dielectric constant and the resistivity measurements discussed above, all reveal characteristic relaxor ferroelectric behavior.[19,27] Moreover, the characteristic temperatures derived from the three different methods are well consistent, which provides solid evidence for the presence of relaxor ferroelectricity in our ZnO−Co nanocomposite thin films.

We have already demonstrated that the Co-implanted ZnO reveals superparamagnetism as well as relaxor ferroelectricity. We now focus on the fact that the electric dipole moments are introduced by the local distortion, which results from the Co implantation. As a consequence, glassy states will appear both electrically and magnetically. Here, their direct magnetoelectric coupling is demonstrated by the $P-E$ hysteresis loop measured at different applied magnetic fields below the freezing temperature. From Figure 6b, one can see that the $P-E$ hysteresis loop becomes slimmer when the applied magnetic field increases up to 7 T. In Figure 6c, we plot the evolution of the remanent polarization and the saturation polarization as a function of the applied magnetic field. Both polarizations decrease with increasing the magnetic field. The relative change of the remanent polarization goes up to 23% at a magnetic field of 7 T. Note that the change of polarization observed here cannot be due to the magnetoresistance (MR) effect.

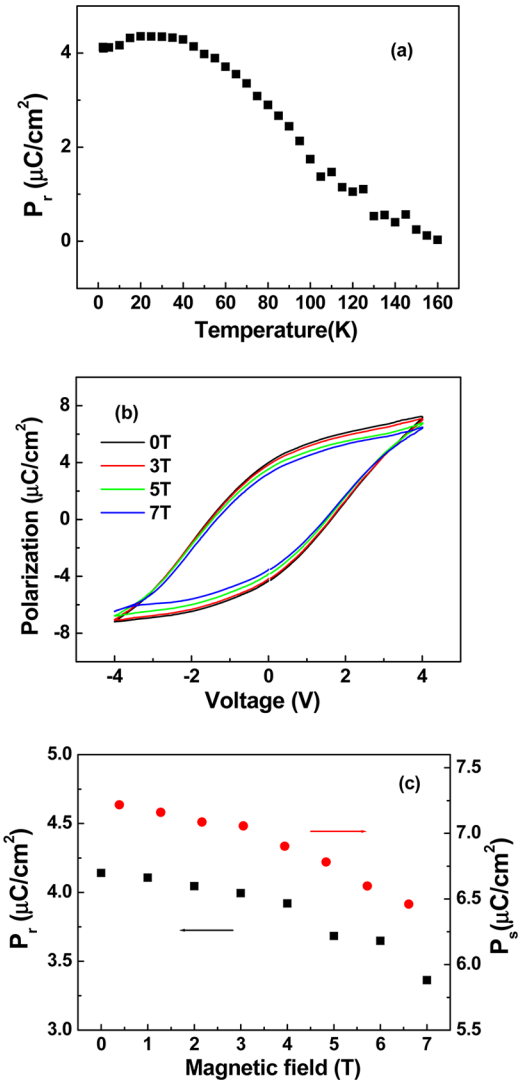

Figure 6. (a) Temperature-dependent remanent polarization of the Co-implanted ZnO thin films. (b) *P*–*E* hysteresis loop at different magnetic fields at 5 K. (c) Evolution of the remanent polarization (black) and saturation polarization (red) as a function of the applied magnetic field at 5 K.

Comparing Figure 5 with Figure 6a, one can see that the polarization remains almost constant while the relative change of resistivity is up to 122% from 15 K down to 2.5 K. We therefore conclude that the change of resistivity due to the MR effect (with a maximum 5.5% at 5 K, data not shown) will not influence the polarization. Although the magnetoelectric coupling appears to be prominent, identifying its origin is, however, not straightforward.

Strain between the (Zn,Co)O matrix and the Co NPs caused by magnetostriction of the Co is unlikely to account for the observed coupling because the magnetostriction is expected to saturate at a field much smaller than 7 T. It has been proposed that the onset of ferromagnetic order will enhance the reorientational mobility of the polar entities in the relaxor ferroelectric $CdCr_2S_4$.[31] This may provide an explanation for the slimmer shape of the polarization loop in an applied magnetic field, as observed in our case. The increase of the reorientational mobility of the dipoles in the presence of a magnetic field will reduce the remanent polarization when removing the applied electrical field. Furthermore, since the electric dipoles are introduced by the disorder resulting from the Co implantation, it is reasonable to assume that the electric dipoles are in the direct neighborhood of the Co NPs and the evenly distributed Co atoms. As we discussed above, the electric dipoles polarize the surrounding medium which is magnetic and form networks of PNRs. These PNRs can therefore respond to the magnetic field as well. As a consequence, when a magnetic field is applied, the electric barrier between the dipoles is lowered probably by a spin-dependent hopping mechanism.[18] The dipoles become more rotatable and less stable, resulting in the observed decrease of the remanent polarization and the saturation polarization in the presence of a magnetic field.

Finally, it should be pointed out that additional post annealing on the ZnO–Co thin films removes the relaxor ferroelectricity. Post annealing is expected to reduce the crystalline disorder. This again supports our conclusion that high-fluence ion implantation induces a certain level of disorder, which results in electric dipoles embedded in the (Zn,Co)O matrix.

4. CONCLUSION

In conclusion, we sucessfully synthesized (Zn,Co)O thin films with embedded crystalline Co nanoparticles by combination of pulsed laser deposition of ZnO and Co ion implantation. The nanocomposite system simultaneously reveals the presence of superparamagnetism and relaxor ferroelectricity. Magneto-electric coupling is demonstrated as well and can be attributed to the interaction between the electric dipole moments and the magnetic moments, which are both induced by the incorporation of Co. Our ZnO–Co thin films are different from conventional strain-mediated composites and can be a good alternative candidate for multiferroic nanocomposites.

■ ASSOCIATED CONTENT

Supporting Information

XRD of a ZnO and a Co-implanted ZnO thin film. Bright field TEM image of a Co-implanted ZnO thin film and the corresponding elemental maps. Energy-dispersive X-ray spectroscopy line scans of a Co-implanted ZnO thin film. ρ as a function of $T^{-3/2}$ at high temperatures and $\ln(\rho)$ as a function of $1/T^{1/4}$ at low temperatures. This material is available free of charge via the Internet at http://pubs.acs.org.

■ AUTHOR INFORMATION

Corresponding Author

*E-mail: yujia.zeng@fys.kuleuven.be.

Notes

The authors declare no competing financial interest.

■ ACKNOWLEDGMENTS

This work has been supported by the Research Foundation – Flanders (FWO, Belgium) as well as by the Flemish Concerted Research Action (GOA/09/006 + GOA/14/007) research program. The X-ray absorption measurements were supported by the FWO Big Science project G.0c12.13. The authors thank D. Szöcs and H. Modarresi for their help in the X-ray absorption measurements.

■ REFERENCES

(1) Ramesh, R.; Spaldin, N. Multiferroics: Progress and Prospects in Thin Films. *Nat. Mater.* **2007**, *6*, 21–29.

(2) Eerenstein, W.; Mathur, N. D.; Scott, J. F. Multiferroic and Magnetoelectric Materials. *Nature* **2006**, *442*, 759−765.
(3) Lottermoser, T.; Lonkai, T.; Amann, U.; Hohlwein, D.; Ihringer, J.; Fiebig, M. Magnetic Phase Control by an Electric Field. *Nature* **2004**, *430*, 541−544.
(4) Kimura, T.; Goto, T.; Shintani, H.; Ishizaka, K.; Arima, T.; Tokura, T. Magnetic Control of Ferroelectric Polarization. *Nature* **2003**, *426*, 55−58.
(5) Hur, N.; Park, S.; Sharma, P. A.; Ahn, J. S.; Guha, S.; Cheong, S.-W. Electric Polarization Reversal and Memory in a Multiferroic Material Induced by Magnetic Fields. *Nature* **2004**, *429*, 392−395.
(6) Prellier, W.; Singh, M. P.; Murugavel, P. The Single-Phase Multiferroic Oxides: from Bulk to Thin Film. *J. Phys.: Condens. Matter* **2005**, *17*, R803−R832.
(7) Lawes, G.; Srinivasan, G. Introduction to Magnetoelectric Coupling and Multiferroic Films. *J. Phys. D: Appl. Phys.* **2011**, *44* (243001), 1−22.
(8) Khomskii, D. Classifying Multiferroics: Mechanisms and Effects. *Physics* **2009**, *2* (20), 1−8.
(9) Martin, L. W.; Crane, S. P.; Chu, Y.-H.; Holcomb, M. B.; Gajek, M.; Huijben, M.; Yang, C.-H.; Balke, N.; Ramesh, R. Multiferroics and Magnetoelectrics: Thin Films and Nanostructures. *J. Phys.: Condens. Matter* **2008**, *20* (434220), 1−13.
(10) Catalan, G.; Scott, J. F. Physics and Applications of Bismuth Ferrite. *Adv. Mater.* **2009**, *21*, 2463−2485.
(11) Vaz, C. A. F.; Hoffman, J.; Ahn, C. H.; Ramesh, R. Magnetoelectric Coupling Effects in Multiferroic Complex Oxide Composite Structures. *Adv. Mater.* **2010**, *22*, 2900−2918.
(12) Zheng, H.; Wang, J.; Lofland, S. E.; Ma, Z.; Mohaddes-Ardabili, L.; Zhao, T.; Salamanca-Riba, L.; Shinde, S. R.; Ogale, S. B.; Bai, F.; et al. Multiferroic $BaTiO_3$-$CoFe_2O_4$ Nanostructures. *Science* **2004**, *303*, 661−663.
(13) Nan, C. W.; Bichurin, M. I.; Dong, S. X.; Viehland, D.; Srinivasan, G. Multiferroic Magnetoelectric Composites: Historical Perspective, Status, and Future Directions. *J. Appl. Phys.* **2008**, *103* (031101), 1−35.
(14) Hill, N. A. Why Are There so Few Magnetic Ferroelectrics? *J. Phys. Chem. B* **2000**, *104*, 6694−6709.
(15) Özgür, Ü.; Alivov, Ya. I.; Liu, C.; Teke, A.; Reshchikov, M. A.; Doğan, S.; Avrutin, V.; Cho, S.-J.; Morkoç, H. A Comprehensive Review of ZnO Materials and Devices. *J. Appl. Phys.* **2005**, *98* (041301), 1−103.
(16) Wang, Z. L. Piezotronic and Piezophototronic Effects. *J. Phys. Chem. Lett.* **2010**, *1*, 1388−1393.
(17) Zeng, Y. J.; Pereira, L. M. C.; Menghini, M.; Temst, K.; Vantomme, A.; Locquet, J.-P.; Van Haesendonck, C. Tuning Quantum Corrections and Magnetoresistance in ZnO Nanowires by Ion Implantation. *Nano Lett.* **2012**, *12*, 666−672.
(18) Li, D. Y.; Zeng, Y. J.; Pereira, L. M. C.; Batuk, D.; Hadermann, J.; Zhang, Y. Z.; Ye, Z. Z.; Temst, K.; Vantomme, A.; Van Bael, M. J.; et al. Anisotropic Magnetism and Spin-Dependent Transport in Co Nanoparticle Embedded ZnO Thin Films. *J. Appl. Phys.* **2013**, *114* (033909), 1−6.
(19) Samara, G. A. The Relaxational Properties of Compositionally Disordered ABO_3 Perovskites. *J. Phys.: Condens. Matter* **2003**, *15*, R367−R411.
(20) Cross, L. E. Relaxor Ferroelectrics. In *Piezoelectricity*; Heywang, W., Lubitz, K., Wersing, W., Eds.; Springer Series in Materials Science; Springer: Berlin, **2008**; Vol. *114*, pp 131−155.
(21) Zhang, S. J.; Li, F. High Performance Ferroelectric Relaxor-$PbTiO_3$ Single Crystals: Status and Perspective. *J. Appl. Phys.* **2012**, *111* (031301), 1−50.
(22) Kutnjak, Z.; Petzelt, J.; Blinc, R. The Giant Electromechanical Response in Ferroelectric Relaxors as a Critical Phenomenon. *Nature* **2006**, *441*, 956−959.
(23) Pereira, L. M. C.; Araújo, J. P.; Van Bael, M. J.; Temst, K.; Vantomme, A. Practical limits for detection of ferromagnetism using highly sensitive magnetometry techniques. *J. Phys. D Appl. Phys.* **2011**, *44* (215001), 1−10.
(24) Zeng, Y. J.; Menghini, M.; Li, D. Y.; Lin, S. S.; Ye, Z. Z.; Hadermann, J.; Moorkens, T.; Seo, J. W.; Locquet, J.-P.; Van Haesendonck, C. Unexpected optical response of single ZnO nanowires probed using controllable electrical contacts. *Phys. Chem. Chem. Phys.* **2011**, *13*, 6931−6935.
(25) Segura-Ruiz, J.; Martínez-Criado, G.; Chu, M. H.; Geburt, S.; Ronning, C. Nano-X-ray Absorption Spectroscopy of Single Co-Implanted ZnO Nanowires. *Nano Lett.* **2011**, *11*, 5322−5326.
(26) Blundell, S. *Magnetism in Condensed Matter*; Oxford University Press: Oxford, 2001.
(27) Cowley, R. A.; Gvasaliya, S. N.; Lushnikov, S. G.; Roessli, B.; Rotaru, G. M. Relaxing with Relaxors: a Review of Relaxor Ferroelectrics. *Adv. Phys.* **2011**, *60*, 229−327.
(28) Rirc, R.; Blinc, R. Vogel-Fulcher Freezing in Relaxor Ferroelectrics. *Phys. Rev. B* **2007**, *76* (020101(R)), 1−3.
(29) Saslow, W. M. Scenario for the Vogel-Fulcher "Law". *Phys. Rev. B* **1988**, *37*, 676−678.
(30) Mott, N. F. Conduction in Glasses Containing Transition Metal Ions. *J. Non-Cryst. Solids* **1968**, *1*, 1−17.
(31) Hemberger, J.; Lunkenheimer, P.; Fichtl, R.; Krug von Nidda, H.-A.; Tsurkan, V.; Loidl, A. Relaxor Ferroelectricity and Colossal Magnetocapacitive Coupling in Ferromagnetic $CdCr_2S_4$. *Nature* **2005**, *434*, 364−367.